JOURNAL OF GUIDANCE, CONTROL, AND DYNAMICS
Vol. 37, No. 3, May–June 2014

Nonlinear Proportional-Derivative Control Incorporating Closed-Loop Control Allocation for Spacecraft

Qinglei Hu* and Bo Li*
Harbin Institute of Technology, Heilongjiang 150001, People's Republic of China
and
Youmin Zhang†
Concordia University, Montreal, Quebec H3G 1M8, Canada

DOI: 10.2514/1.61815

A novel saturated proportional-derivative control law incorporated with closed-loop control allocation is proposed for spacecraft attitude stabilization in this paper. More specifically, a saturated proportional-derivative-based baseline nonlinear controller is designed to guarantee the globally asymptotic stability under control input/signal constraints. Then, a closed-loop constrained optimal control allocation scheme is employed to distribute the moments synthesized by the baseline controller over the redundant actuators in the presence of constraints due to actuator amplitude and rate constraints. The optimal control solution is to be found by penalizing the control allocation errors and rates using optimal quadratic programming algorithms. A significant feature of this work is that the asymptotic stability with the closed-loop control allocation is guaranteed theoretically. Simulation results are presented to illustrate the performance of the proposed scheme.

I. Introduction

ACCURATE and reliable attitude stabilization is one of the most important problems and widely studied applications in current spacecraft attitude control system design. For orbiting spacecraft, dynamics are strongly nonlinear in nature and are also affected by various disturbances from the environment that influence the mission objectives significantly. In addition, actuator uncertainties induced by misalignment during installation and torque magnitude measurement errors further increase the design complexity and difficulty. In practice, due to physical limitations on actuators, the virtual control signals or commanded actuator torques synthesized by the controller could exceed actuators' physical limits, which may lead to actuators' saturation. This can induce serious discrepancies between commanded control signals and actually executed control efforts. All of these in a realistic environment cause considerable difficulties and challenges in the design of an attitude control system of spacecraft for meeting high-precision pointing requirements and desired control performance during the missions, especially when all these issues have to be handled simultaneously.

Recently, many studies related to attitude control law design have been reported in literature based on several inspiring approaches, such as optimal control [1], nonlinear feedback control [2,3], adaptive control [4], and robust control or their integration [5–7]. Generally speaking, most or part of the previous works can deal with external disturbances and uncertainties to a certain degree, but can hardly be applied to the practical application. In view of its simplicity and good performance for practical applications, proportional-derivative (PD) or PD-like controls have been extensively studied as well. In [8,9], Tsiotras shows that there exists a simple linear asymptotically stabilizing PD control law for the attitude motion of a rigid body. Using a unit quaternion model and angular velocity in a feedback controller, the attitude stabilization issue has also been investigated by many researchers [10–12]. It should be noted that the actuators are required to produce large and fast enough joint torques in these control methods, although this will hardly be achieved due to limited magnitude and slew rate constraints in practical actuators. By recognizing this problem, several solutions have been presented to deal with actuator saturation constraints. In [13], Ali et al. designed a nonlinear bounded control using a backstepping method and an inverse tangent-based tracking function. Boskovic et al. [14] also proposed two globally stable control algorithms for robust stabilization of spacecraft in which the input saturation is considered using explicit saturation function. Su and Zheng [15] presented a simple saturated PD control by introducing the standard hypertangent function, and the globally asymptotic stabilization of a rigid spacecraft can be guaranteed. In [16], a smooth global stabilization saturated attitude control law has also been derived, from which known limits on the control authority of the system are rigorously enforced.

Generally, modern spacecraft often use redundant actuators for enhanced reliability and safety to achieve reliable orbiting operation. That is to say, the spacecraft is then an overactuated system, and there are freedoms to design the control systems by making use of the existing hardware redundancy due to the overactuated actuators. To make effective use of these hardware actuator redundancies, the control allocation (CA) technique is one natural and necessary solution for achieving a desired control objective by distributing appropriately the lower dimension of the total control signals synthesized by the baseline controller to each individual actuator among the higher-dimension redundant actuators. Control allocation techniques have been extensively investigated in the last decades, such as daisy chaining [17], linear or nonlinear programming-based optimization algorithms [18], direct allocation [18,19], and dynamic control allocation [19–22]. Fault-tolerant control strategies combining control allocation or control reallocation techniques have also been investigated recently [23–26]. However, most of the preceding control allocation schemes are studied and worked as an open-loop system in some sense, and the stability/stabilization issue of a closed-loop system under combination of control allocation with the baseline controller is not considered [27,28] due to the inherent difficulty for such a control design task. There are few research works available in this related area. As a few early attempts along this line, a sufficient asymptotic stability condition for the zero dynamics of systems with daisy chain control allocation was given initially by Buffington and Enns [17], and more common control allocation methods were presented by Buffington et al. in [18]. In [28], a closed-loop control allocation system based on the cascaded generalized inverse method is established and a necessary sufficient condition for the stability of the satellite system is presented.

Received 21 January 2013; revision received 23 September 2013; accepted for publication 23 September 2013; published online 21 March 2014.

*Department of Control Science and Engineering, Harbin.
†Department of Mechanical and Industrial Engineering; Youmin.Zhang@concordia.ca. Senior Member AIAA.

In this work, an attempt or innovation is made to provide a simple saturated proportional-derivative (SPD) control strategy incorporating a close-loop constrained optimal control allocation (CLCA) scheme for spacecraft attitude stabilization in the presence of control input/signal constraints with respect to the actuator amplitude and rate constraints. More specifically, the SPD control law will be used for achieving the desired control commands under control input/signal constraints, and closed-loop CA will be used for dealing with the problem of distributing the total virtual control command synthesized by the SPD controller into each individual actuator properly by using extended optimal quadratic programming algorithms and by taking into account the constraints due to actuator amplitude and rate constraints. It should be noted that the important point and contribution of this work is that asymptotical stability of the closed-loop system with the designed SPD baseline controller and the CA scheme can be guaranteed. The key features/achievements of the designed control scheme are that it ensures 1) asymptotical stability of the closed-loop system, 2) convergence of both attitude and bounded control torques, and 3) simple design procedure and structure of the proposed scheme. The feature of simple design and structure is of great interest for aerospace industry with real-time implementation when onboard computing power is limited. The benefits of the proposed control method are analytically authenticated and also validated via simulation studies.

The paper is organized as follows. Section II states spacecraft modeling and control problem formulation. An attitude control law design by combining an SPD baseline control law and a novel control allocation scheme under actuator constraints is presented in Sec. III. Numerical simulation results are presented in Sec. IV to demonstrate various features of the proposed control scheme. Finally, the paper is completed with some concluding comments.

II. Spacecraft Modeling and Control Problem Formulation

In this section, the mathematical model of a rigid spacecraft is briefly presented. The nonlinear equations of the attitude motions, in terms of components along the body-fixed reference frame, are given by the spacecraft kinematics and the attitude dynamics as follows.

A. Spacecraft Kinematics

In this paper, the orientation of the body with respect to the inertial frame will be represented in the form of modified Rodrigues parameters (MRPs). The kinematic equation in terms of MRPs is [15]

$$\dot{\boldsymbol{\rho}} = \boldsymbol{G}(\boldsymbol{\rho})\boldsymbol{\omega} \quad \text{with} \quad \boldsymbol{G}(\boldsymbol{\rho}) \triangleq \frac{1}{2}\left(\boldsymbol{I} - \boldsymbol{S}(\boldsymbol{\rho}) + \boldsymbol{\rho}\boldsymbol{\rho}^T - \frac{1+\boldsymbol{\rho}^T\boldsymbol{\rho}}{2}\boldsymbol{I}\right) \tag{1}$$

where $\boldsymbol{I}$ represents an identity unit matrix with corresponding dimensions. The MRPs are defined as $\boldsymbol{\rho}_i = q_i/(1+q_0)$ with $\bar{\boldsymbol{q}} = [q_0\ \boldsymbol{q}^T]^T \in \mathbb{R}\times\mathbb{R}^3$ representing spacecraft quaternions, and $\boldsymbol{q} = [q_1, q_2, q_3]^T$ with $i = 1, 2, 3$. MRPs are $\boldsymbol{\rho} = [\rho_1, \rho_2, \rho_3]^T$. The angular velocity vector with respect to the inertial frame is $\boldsymbol{\omega} \in \mathbb{R}^{3\times 1}$. $\boldsymbol{S}(\cdot)$ denotes a skew-symmetric matrix given by

$$\boldsymbol{S}(\boldsymbol{\rho}) = \begin{bmatrix} 0 & -\rho_3 & \rho_2 \\ \rho_3 & 0 & -\rho_1 \\ -\rho_2 & \rho_1 & 0 \end{bmatrix} \tag{2}$$

In addition, the matrix $\boldsymbol{G}(\boldsymbol{\rho})$ has the following properties:

$$\boldsymbol{\rho}^T\boldsymbol{G}(\boldsymbol{\rho})\boldsymbol{\omega} = \left(\frac{1+\boldsymbol{\rho}^T\boldsymbol{\rho}}{4}\right)\boldsymbol{\rho}^T\boldsymbol{\omega} \tag{3}$$

If the principal axis and principal angle are considered for rotation, then MRPs have the advantage that it remains valid for eigenaxis rotations up to 360 deg.

B. Spacecraft Dynamics

When all the actuators function normally, the rigid spacecraft dynamics can be given as [15,29]

$$\boldsymbol{J}\dot{\boldsymbol{\omega}}(t) = -\boldsymbol{S}(\boldsymbol{\omega}(t))\boldsymbol{J}\boldsymbol{\omega}(t) + \boldsymbol{u}(t) \tag{4}$$

where $\boldsymbol{J} \in \mathbb{R}^{3\times 3}$ is the total inertia matrix of the spacecraft, which is a positive-definite symmetrical matrix. The control torque vector is denoted by $\boldsymbol{u}(t) = [\,u_1 \quad u_2 \quad u_3\,]^T \in \mathbb{R}^3$.

C. Control Objective

Consider the spacecraft attitude control system given by Eqs. (1) and (4) under the preceding reasonable assumptions. Design a control input $\boldsymbol{u}(t) \in \boldsymbol{\Omega}_u$ such that, for all physically realizable initial conditions, the states of the closed-loop system are globally asymptotically stable, which can be expressed as follows:

$$\lim_{t\to\infty}\boldsymbol{\rho}(t) = 0, \qquad \lim_{t\to\infty}\boldsymbol{\omega}(t) = 0$$

III. Attitude Control Law Design

In view of exploiting available actuator hardware redundancy for effective attitude control system design, attitude control law design in this paper will use the principle of baseline controller and control allocation framework with the following two design steps [18]: 1) design a control law specifying which total control effort to be produced (net torques, etc.), known as virtual control law or baseline control law; and 2) design a control allocation scheme (or control allocator) that maps the total control demand determined by the baseline control law onto individual actuator settings (such as reaction wheel torques, etc.), as shown in Fig. 1.

Assumption 1: Because of physical limitations on the actuators in spacecraft, it is assumed that actuator output torques have the same constraint value $\tau_{\max}$ for simplicity, that is,

$$\boldsymbol{\tau}(t) \in \boldsymbol{\Omega}_\tau := \{\boldsymbol{\tau} \in \mathbb{R}^m \,||\tau_i| \le \tau_{\max}, i = 1, 2, \ldots, m\} \tag{5}$$

where m is the number of actuators considered. With respect to the physical saturation limits of actuators, it is also assumed that the virtual control signals designed from the control law ought to be subject to the following constraint:

$$\boldsymbol{u}(t) \in \boldsymbol{\Omega}_u := \{\boldsymbol{u} \in \mathbb{R}^n \,||u_i| \le u_{\max}, i = 1, 2, \ldots, n\} \tag{6}$$

where $n (n < m)$ is the number of control inputs/signals to be sent to actuators and typically $n = 3$ as defined in Eq. (4), whereas the overactuated actuators configuration normally used for spacecraft and considered in this paper is $m = 4$, as will be illustrated later. The maximum magnitude of the control signals $u_{\max}$ can be determined by the physical saturation limitations on available overactuated actuators. Note that, in the case that $n = m$, there will be no redundant

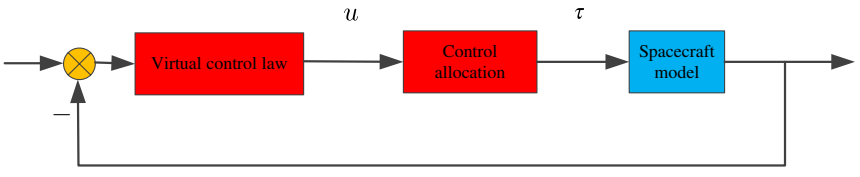

Fig. 1 Block diagram for spacecraft attitude control system with baseline control law and control allocation modules.

actuators and $u_{\max}$ will be the same as $\tau_{\max}$, and then the CA module shown in Fig. 1 will become not necessary, and the spacecraft attitude control problem will then become a conventional control system design with only baseline controller needs to be designed.

A. Saturated Proportional-Derivative-Based Virtual/Baseline Control Law Design

Based on the control structure specified in Fig. 1, an equivalent representation of Eq. (4) can be written as

$$\boldsymbol{J}\dot{\boldsymbol{\omega}}(t) = -\boldsymbol{S}(\boldsymbol{\omega}(t))\boldsymbol{J}\boldsymbol{\omega}(t) + \boldsymbol{u}(t) \tag{7a}$$

$$\boldsymbol{u}(t) = \boldsymbol{D}\boldsymbol{\tau}(t) \tag{7b}$$

where the distribution matrix $\boldsymbol{D} \in \mathbb{R}^{3\times m}$ is used to describe distribution of the physical actuators for representing the influence of each actuator on the angular acceleration of the spacecraft, which is dependent on the physical configuration and overall system design of the overactuated spacecraft based on the mission requirement, and the full row rank of $\boldsymbol{D}$ is required to guarantee that the overactuated attitude system is controllable in normal/fault-free cases.

In what follows, such an attitude control law for spacecraft as given in Eqs. (1) and (4) will be developed to achieve the control objective given in the subsequent section. For the following controller design, it is assumed that these states $\boldsymbol{\rho}(t)$ and $\boldsymbol{\omega}(t)$ can be obtained accurately from some measuring elements installed on the orbiting spacecraft.

Motivated by the work given in [15], the first main result of this paper is summarized and presented as the following theorem.

Theorem 1: Given the spacecraft attitude stabilization control system modeled by Eqs. (1) and (4), there exists controller gains β and $\alpha(t)$ to ensure that the system is globally asymptotically stable under the following SPD control law:

$$\boldsymbol{u}(t) = -(1-\beta)u_{\max}\,\mathrm{Tanh}(\boldsymbol{\omega}(t)/\alpha^2(t)) - \beta u_{\max}\frac{\boldsymbol{\rho}}{\sqrt{1+\boldsymbol{\rho}^T\boldsymbol{\rho}}} \tag{8}$$

where β is a constant control gain with $\beta \in [0, 1]$, $\alpha^2(t)$ is a strictly bounded above-zero scalar sharpness function [16] that governs the magnitude of the control rates, and $0 < \alpha_{\min}^2 \le \alpha^2(t) \in L_\infty, \dot{\alpha} \in L_\infty$. Note that the control signal upper/lower limit is represented by a proper bound value of $u_{\max}$ in magnitude and the virtual control torques are subject to (s.t.) the control signal constraints specified in Eq. (6). In addition, vector $\mathrm{Tanh}(\boldsymbol{\omega}(t)) \in \mathbb{R}^3$ is defined as

$$\mathrm{Tanh}(\boldsymbol{\omega}(t)) \triangleq [\,\tanh(\omega_1(t)) \quad \tanh(\omega_2(t)) \quad \tanh(\omega_3(t))\,]^T$$

where $\mathrm{Tanh}(\cdot)$ denotes the standard hyperbolic tangent function.

Proof: Considering the following Lyapunov function candidate

$$V = \frac{1}{2}\boldsymbol{\omega}^T\boldsymbol{J}\boldsymbol{\omega} + 4\beta u_{\max}\left(1 - \frac{1}{\sqrt{1+\boldsymbol{\rho}^T\boldsymbol{\rho}}}\right) \tag{9}$$

where t is dropped from $\boldsymbol{\omega}(t)$ and $\alpha^2(t)$ for brevity in the following derivation and

$$1 - \frac{1}{\sqrt{1+\boldsymbol{\rho}^T\boldsymbol{\rho}}} \ge 0$$

is obviously guaranteed.

Differentiation of V with respect to time and with the system dynamics (4) and the control law (8) yields

$$\begin{aligned}\dot{V} &= \boldsymbol{\omega}^T\boldsymbol{J}\dot{\boldsymbol{\omega}} + 4\beta u_{\max}\left(\frac{\boldsymbol{\rho}^T\dot{\boldsymbol{\rho}}}{(1+\boldsymbol{\rho}^T\boldsymbol{\rho})\sqrt{1+\boldsymbol{\rho}^T\boldsymbol{\rho}}}\right)\\ &= \boldsymbol{\omega}^T\boldsymbol{u} + \beta u_{\max}\boldsymbol{\omega}^T\frac{\boldsymbol{\rho}}{\sqrt{1+\boldsymbol{\rho}^T\boldsymbol{\rho}}} = -(1-\beta)u_{\max}\boldsymbol{\omega}^T\,\mathrm{Tanh}(\boldsymbol{\omega}/\alpha^2)\end{aligned}$$

Because $\boldsymbol{\omega}^T\,\mathrm{Tanh}(\boldsymbol{\omega}/\alpha^2) \ge 0$ is always guaranteed for all $\boldsymbol{\omega}$ from the property of the standard hyperbolic tangent function, one can obtain

$$\dot{V} = -(1-\beta)u_{\max}\boldsymbol{\omega}^T\,\mathrm{Tanh}(\boldsymbol{\omega}/\alpha^2) \le 0 \tag{10}$$

which implies that V and $\boldsymbol{\omega}$ are bounded for all time.

Integrating both sides of Eq. (10) with respect to time, one can obtain

$$V_\infty - V_0 = -(1-\beta)u_{\max}\int_0^\infty \boldsymbol{\omega}^T\,\mathrm{Tanh}(\boldsymbol{\omega}/\alpha^2)\,\mathrm{d}t \le 0$$

where the symbols

$$V_\infty = \lim_{t\to\infty} V(t) \quad \text{and} \quad V_0 = V(0)$$

are used for brevity. Because the term $\boldsymbol{\omega}^T\,\mathrm{Tanh}(\boldsymbol{\omega}/\alpha^2) \ge 0$ is uniformly continuous and

$$\int_0^\infty \boldsymbol{\omega}^T\,\mathrm{Tanh}(\boldsymbol{\omega}/\alpha^2)\,\mathrm{d}t$$

is finite, Barbalat's lemma dictates that $\boldsymbol{\omega}$ converges to the origin, that is,

$$\lim_{t\to\infty}\boldsymbol{\omega}(t) = 0$$

Since $\dot{V} \equiv 0$ means that $\boldsymbol{\omega} \equiv 0$, from the closed-loop system formed by Eqs. (1) and (4), one has $\boldsymbol{\rho} \equiv 0$. Using LaSalle's invariance principle [11], one can obtain that the closed-loop attitude system of the rigid spacecraft is globally asymptotically stable.

Remark 1: Using the property of the standard hyperbolic tangent function and the fact that

$$\left|\frac{x_i}{\sqrt{1+\boldsymbol{x}^T\boldsymbol{x}}}\right| \le 1, \qquad i = 1, 2, 3$$

where $\boldsymbol{x}$ represents $\boldsymbol{\rho}$ in the SPD control law in Eq. (8), along with the chosen bounds on the parameter β for ensuring that the SPD control law satisfies the control input/signal constraints specified in Eq. (6) and finally actuator saturation constraints specified in Eq. (5). Therefore, a name of SPD nonlinear control law in view of both the attitude P and velocity D variables and following explicit saturation constraints S are all considered in such a nonlinear control law formulation:

$$\begin{aligned}|u_i| &\le |(1-\beta)u_{\max}\,\mathrm{Tanh}(\boldsymbol{\omega}_i/\alpha^2)| + \left|\beta u_{\max}\frac{\boldsymbol{\rho}_i}{\sqrt{1+\boldsymbol{\rho}^T\boldsymbol{\rho}}}\right|\\ &\le |(1-\beta)u_{\max}| + |\beta u_{\max}| \le u_{\max}\end{aligned} \tag{11}$$

Then, the control input saturation avoidance can be guaranteed by selecting a proper value of $u_{\max}$, which is determined by the physical saturation limitations on available overactuated actuators.

B. Closed-Loop Control Allocation Design with Optimization Method

From the preceding analysis, even if the attitude stabilization target can be achieved by virtual control law (8), other practical problems, such as energy saving (minimizing energy consumption), capability for final actuator saturation avoidance against actuator amplitude, and rate saturation limits, although a bound as defined in Eq. (6) has been considered in the design of the baseline controller using Eq. (8), etc., should be taken into account for simultaneous control system design. Control allocation is necessary and useful for the control of overactuated systems, including spacecraft systems. It deals with distributing the desired total control command determined by the virtual control law equivalently to the individual overactuated actuators for achieving the commended maneuvering specified by the virtual control law. Generally, the CA problem is formulated as an

optimization problem, which systematically handles redundant sets of actuators, actuator constraints and power consumption minimization, wear/tear, and other undesirable effects. Because it is a practical and powerful approach for solving control problems for systems with overactuated actuators, there is extensive literature on CA that discuss different algorithms, approaches, and applications. Page and Steinberg in [27] compare the closed- and open-loop performance of 16 different control allocation algorithms. Bodson provides a comprehensive evaluation of different constrained numerical optimization methods for control allocation in [30]. Using CA, the actuator selection task is separated from the regulation (baseline control design) task in the overall control system design. Common sense in the early stage of study for CA combining baseline/virtual control assumes that there is no effect of the stability of the overall closed-loop system based on such a separated design for the baseline controller and control allocator because the closed-loop system's stability is mainly guaranteed by the baseline controller [19,24]. Such common sense, in fact, was based on the assumption that the control allocation scheme does not affect system stability, which also implied the inherent stability of the control allocator. Such an assumption is, in fact, not valid and must be approved in a similar way as the stability issue with baseline controller for a closed-loop system. This is the main motivation of the work to be presented in this paper for designing a control system with an integrated baseline control and control allocation scheme with guaranteed stability of the overall closed-loop system. For such a purpose and as a further extension to several existing works that consider the closed-loop system stability analysis [17,27,28,31], in which the stability/stabilization issue of the overall closed-loop system under the combination of control allocation with the baseline controller is still an unsolved or at least not well solved problem, a new dynamic control allocation scheme using a constrained optimal quadratic programming is developed in this study in an effort to provide an overall closed-loop system stability guarantee with the combined baseline control law designed in Eq. (8) based on the SPD nonlinear control. The idea of the system stability guarantee for entire/overall closed-loop system is to be achieved 1) with the stability guarantee of the closed-loop system without consideration of overactuated actuators and, therefore, the preceding SPD controller is proposed in this work, and 2) the stability guarantee of the CA part is achieved by the proposed closed-loop CA scheme to be presented in this section. The developed control allocation scheme and proof of the overall closed-loop system stability guarantee will be presented at a later time.

Considering the actuator amplitude and rate constraints and defining the following compact set for each reaction wheel as

$$\boldsymbol{\Omega}_1 = \{\boldsymbol{\tau}_i \in \mathbb{R}^m | \tau_{\min} \le \tau_i \le \tau_{\max}, i = 1, 2, 3, \ldots, m\} \tag{12a}$$

$$\boldsymbol{\Omega}_2 = \{\dot{\tau}_i \in \mathbb{R}^m | \eta_{\min} \le \dot{\tau}_i \le \eta_{\max}, i = 1, 2, 3, \ldots, m\} \tag{12b}$$

where $\tau_{\min}$ and $\tau_{\max}$ are the lower and upper actuator amplitude limitations, $\eta_{\min}$ and $\eta_{\max}$ denote the minimal and maximal actuator rate limitations, respectively.

Because the control allocator is part of a digital control system, it is reasonable to approximate the time derivative as

$$\dot{\boldsymbol{\tau}}(t) \approx \frac{\boldsymbol{\tau}(t) - \boldsymbol{\tau}(t-T)}{T} \tag{13}$$

where T is the sampling time, and $\boldsymbol{\tau}(t-T)$ is the control torques in the previous sampling instant. Then one can get the overall actuator constraints as

$$\underline{\boldsymbol{\tau}}(t) \le \boldsymbol{\tau}(t) \le \bar{\boldsymbol{\tau}}(t) \tag{14}$$

with $\underline{\tau}_i(t) = \max\{\tau_i(t)_{\min}, \tau_i(t-T) + T\min\{\eta_{\min}\}\}$ and $\bar{\tau}_i(t) = \min\{\tau_i(t)_{\max}, \tau_i(t-T) + T\max\{\eta_{\max}\}\}$.

1. *Open-Loop Constrained Optimal Control Allocation Design*

First, for the purpose of comparison with the closed-loop CA scheme to be proposed in next subsection, an open-loop control allocation scheme, such as the pseudoinverse (PI) method [19–21], is studied first with the system block diagram shown in Fig. 2, where $\boldsymbol{D}^{\dagger} = \boldsymbol{D}^T(\boldsymbol{D}\boldsymbol{D}^T)^{-1}$. In view of the aforementioned problem and constraints, the proposed control allocation algorithm can be formulated as a constrained optimal quadratic programming problem as follows:

$$J = \arg\min_{\tau(t)\in\boldsymbol{\Omega}_0}\{\|\boldsymbol{W}_0\boldsymbol{\tau}_{\text{act}}(t)\|^2 + \|\boldsymbol{W}_1[\boldsymbol{\tau}_{\text{act}}(t) - \boldsymbol{\tau}_d(t)]\|^2 + \|\boldsymbol{W}_2[\boldsymbol{\tau}_{\text{act}}(t) - \boldsymbol{\tau}_{\text{act}}(t-T)]\|^2\} \tag{15a}$$

$$\boldsymbol{\Omega}_0 = \arg\min_{\underline{\boldsymbol{\tau}}(t)\le\boldsymbol{\tau}_{\text{act}}(t)\le\bar{\boldsymbol{\tau}}(t)} \|\boldsymbol{u}_d(t) - \boldsymbol{D}\boldsymbol{\tau}_{\text{act}}(t)\| \tag{15b}$$

where $\boldsymbol{W}_0$, $\boldsymbol{W}_1$, and $\boldsymbol{W}_2$ denote relevant diagonal positive-defined weighting matrices, $\boldsymbol{u}_d(t)$ and $\boldsymbol{\tau}_d(t)$ denote the desired system control torques and actuator torques, respectively, and $\boldsymbol{u}_{\text{act}}(t)$ and $\boldsymbol{\tau}_{\text{act}}(t)$ denote the actual system control torques and actuator torques, respectively.

To facilitate for solving the constrained optimal problem, the choice of the elements $\boldsymbol{r}_0$ and $\boldsymbol{r}_1$ in diagonal positive-defined gain matrices $\boldsymbol{R}_0$ and $\boldsymbol{R}_1$ are selected, respectively:

$$\boldsymbol{r}_0 = \begin{cases} \frac{\bar{\boldsymbol{\tau}}_{\text{act}}(t)}{\boldsymbol{\tau}_{\text{act}}(t)} & \boldsymbol{\tau}_{\text{act}}(t) \ge \bar{\boldsymbol{\tau}}_{\text{act}}(t) \\ 1 & \underline{\boldsymbol{\tau}}_{\text{act}}(t) \le \boldsymbol{\tau}_{\text{act}}(t) \le \bar{\boldsymbol{\tau}}_{\text{act}}(t) \\ \frac{\underline{\boldsymbol{\tau}}_{\text{act}}(t)}{\boldsymbol{\tau}_{\text{act}}(t)} & \boldsymbol{\tau}_{\text{act}}(t) \le \underline{\boldsymbol{\tau}}_{\text{act}}(t) \end{cases},$$

$$\boldsymbol{r}_1 = \begin{cases} \frac{\bar{\boldsymbol{\tau}}_d(t)}{\boldsymbol{\tau}_d(t)} & \boldsymbol{\tau}_d(t) \ge \bar{\boldsymbol{\tau}}_d(t) \\ 1 & \underline{\boldsymbol{\tau}}_d(t) \le \boldsymbol{\tau}_d(t) \le \bar{\boldsymbol{\tau}}_d(t) \\ \frac{\underline{\boldsymbol{\tau}}_d(t)}{\boldsymbol{\tau}_d(t)} & \boldsymbol{\tau}_d(t) \le \underline{\boldsymbol{\tau}}_d(t) \end{cases} \tag{16}$$

where the gain matrices can be defined as $\boldsymbol{R}_0 = \text{diag}(\boldsymbol{r}_0)$ and $\boldsymbol{R}_1 = \text{diag}(\boldsymbol{r}_1)$, which is to make the synthesized control torques $\boldsymbol{\tau}_{\text{act}}(t)$ and the desired torques $\boldsymbol{\tau}_d(t)$ in one limited region as defined in Eq. (14), and the more practical advantage of this definition is for solving the constrained optimal problem simply and conveniently.

Accordingly, the optimal quadratic programming problem described by Eq. (15) can then be modified as

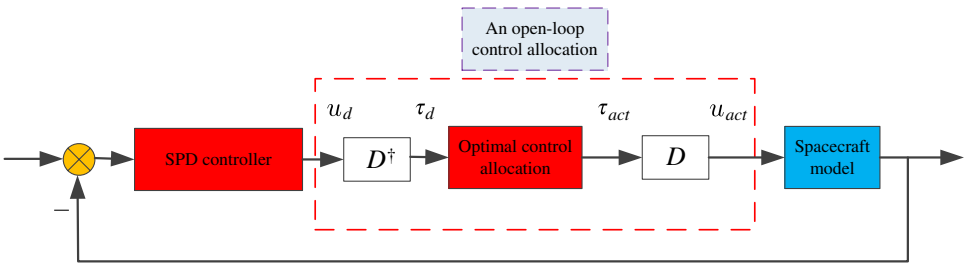

Fig. 2 Block diagram for spacecraft attitude control system with an open-loop control allocation scheme.

$$J = \arg\min_{\tau(t)\in\Omega_0}\{\|\boldsymbol{R}_0\boldsymbol{W}_0\boldsymbol{\tau}_{\text{act}}(t)\|^2 + \|\boldsymbol{R}_1\boldsymbol{W}_1[\boldsymbol{\tau}_{\text{act}}(t) - \boldsymbol{\tau}_d(t)]\|^2 + \|\boldsymbol{W}_2[\boldsymbol{\tau}_{\text{act}}(t) - \boldsymbol{\tau}_{\text{act}}(t-T)]\|^2\}$$
$$\text{s.t. } \boldsymbol{u}_d(t) = \boldsymbol{D}\boldsymbol{\tau}_{\text{act}}(t) \tag{17}$$

To solve this control allocation problem, the following lemma and corollaries will be helpful in the subsequent analysis.

Lemma 1 [32]: For a matrix $\boldsymbol{A} \in \boldsymbol{R}^{m\times n}$, where $m < n$, with rank m, and $m = 3$, $n = 4$ in particular for this work, the minimum norm problem

$$\min_{\boldsymbol{x}} \|\boldsymbol{x}\|_2, \qquad \text{s.t. } \boldsymbol{x} = \boldsymbol{A}\boldsymbol{y}$$

has the solution

$$\boldsymbol{y} = \boldsymbol{A}^{\dagger}\boldsymbol{x}$$

where the symbol † denotes the pseudoinverse operator defined as $\boldsymbol{A}^{\dagger} = \boldsymbol{A}^T(\boldsymbol{A}\boldsymbol{A}^T)^{-1}$.

Corollary 1 [20]: The weighted minimum norm problem

$$\min_{x} \|\boldsymbol{W}(\boldsymbol{x} - \boldsymbol{x}_0)\|_2, \qquad \text{s.t. } \boldsymbol{A}\boldsymbol{x} = \boldsymbol{y}$$

where $\boldsymbol{W}$ is a nonsingular weighting matrix, has the following solution

$$\boldsymbol{x} = \boldsymbol{F}\boldsymbol{x}_0 + \boldsymbol{G}\boldsymbol{y}, \qquad \boldsymbol{F} = \boldsymbol{I} - \boldsymbol{G}\boldsymbol{A}, \qquad \boldsymbol{G} = \boldsymbol{W}^{-1}(\boldsymbol{A}\boldsymbol{W}^{-1})^{\dagger}$$

Corollary 2 [20]: The cost function

$$\min_{x} \|\boldsymbol{W}_1(\boldsymbol{x} - \boldsymbol{x}_1)\|^2 + \|\boldsymbol{W}_2(\boldsymbol{x} - \boldsymbol{x}_2)\|^2$$

has the same minimizing argument as

$$\min_{\boldsymbol{x}} \|\boldsymbol{W}(\boldsymbol{x} - \boldsymbol{x}_0)\|_2$$

where $\boldsymbol{W} = (\boldsymbol{W}_1^2 + \boldsymbol{W}_2^2)^{1/2}$, $x_0 = \boldsymbol{W}^{-2}(\boldsymbol{W}_1^2\boldsymbol{x}_1 + \boldsymbol{W}_2^2\boldsymbol{x}_2)$.

Then, let the preceding lemma and corollaries hold, and the control allocation problem of Eq. (17) has the following solution:

$$\tau_{\text{act}}(t) = \boldsymbol{E}\tau_d(t) + \boldsymbol{F}\tau_{\text{act}}(t-T) + \boldsymbol{G}\boldsymbol{u}_d(t) \tag{18}$$

where $\boldsymbol{W} = ((\boldsymbol{R}_0\boldsymbol{W}_0)^2 + (\boldsymbol{R}_1\boldsymbol{W}_1)^2 + \boldsymbol{W}_2^2)^{1/2}$, $\boldsymbol{E} = (\boldsymbol{I} - \boldsymbol{G}\boldsymbol{D})\boldsymbol{W}^{-2}(\boldsymbol{R}_1\boldsymbol{W}_1)^2$, $\boldsymbol{F} = (\boldsymbol{I} - \boldsymbol{G}\boldsymbol{D})\boldsymbol{W}^{-2}\boldsymbol{W}_2^2$, and $\boldsymbol{G} = \boldsymbol{W}^{-1}(\boldsymbol{D}\boldsymbol{W}^{-1})^{\dagger}$.

In view of Eq. (18), the real actuator torques are the weighted sum of the three types of torques defined earlier. The benefit of this control allocation solution is that decreased effect of the noises or disturbances and high performance can be achieved [22].

Remark 2: Equation (15) is a cost function to be minimized subject to the linear and nonlinear constraints. From this cost function, the total power consumption is represented by the first term in the criterion, in which, if the larger weighting matrix $\boldsymbol{w}_0$ is chosen, the smaller energy consumption will be achieved. For the second term, it is used to minimize the error of the control allocation such that the control torques would be convergent to the desired command quickly when a large weighting matrix $\boldsymbol{w}_1$ is selected. In addition, to minimize the changing rate of the control torques, the third term is chosen such that the response of the actuator will be smooth and steady if one can set a proper weighting matrix $\boldsymbol{w}_2$. In fact, the three terms defined in Eq. (15a) do not contradict each other because these weighting matrixes are used for representing their importance, priority, or weight in this specified overall optimal object function.

2. *Closed-Loop Constrained Optimal Control Allocation Design*

To apply the developed optimal control allocation scheme to a closed-loop system for the purpose of stability guarantee, which is not possible in the preceding open-loop CA scheme, a novel control allocation scheme denoted as closed-loop control allocation is proposed for the spacecraft attitude stabilization control system in this subsection. In fact, similar to control systems with feedback, closed-loop CA is trying to use this powerful and useful concept for guaranteeing the expected distribution of control signals determined by the baseline controller (SPD controller in this work) among redundant actuators and the expected convergence for the stability guarantee. That is to say, the process of $\boldsymbol{u}_{\text{act}} \to \boldsymbol{u}_d$ is stable asymptotically, which is the main result/conclusion in this subsection. This is not possible for open-loop CA because there is no such an internal feedback, although optimization through three weighting functions/matrices has been used for the CA design. The overall system block diagram with details on such a CA with feedback scheme is presented in Fig. 3, in which z^{-1} is a delay or discretization operator and $\boldsymbol{e}$ is the control allocation error of the actuators from the actuator torques before and after the "optimal control allocation" module.

In general, the attitude control problem falls naturally into a control system design with the CA module to be included effectively for a practical overactuated system. Although the stability/stabilization of the baseline controller could be achieved easily and not necessarily using the proposed SPD controller in this paper, such a design framework is problem driven and is not a simple or straightforward combination of existing controllers design for individual baseline control law and control allocation scheme. At the same time, a stability-guaranteed overall system is achieved in this subsection, which has been considered rarely or not been well achieved in most existing works in the field. From this viewpoint, the key result of this overall closed-loop control allocation system is presented as follows.

Theorem 2: For the spacecraft attitude system with closed-loop control allocation as shown in Fig. 3, the closed-loop control allocation system can be described as

$$(\boldsymbol{I} - z^{-1}(\boldsymbol{I} - \boldsymbol{L}))\boldsymbol{U}_{\text{act}}(z) = (\boldsymbol{L} + \boldsymbol{D}\boldsymbol{G} - z^{-1}\boldsymbol{D}\boldsymbol{G})\boldsymbol{U}_d(z) + \boldsymbol{D}\boldsymbol{F}z^{-1}(1 - z^{-1})\boldsymbol{\Gamma}_{\text{act}}(z) \tag{19}$$

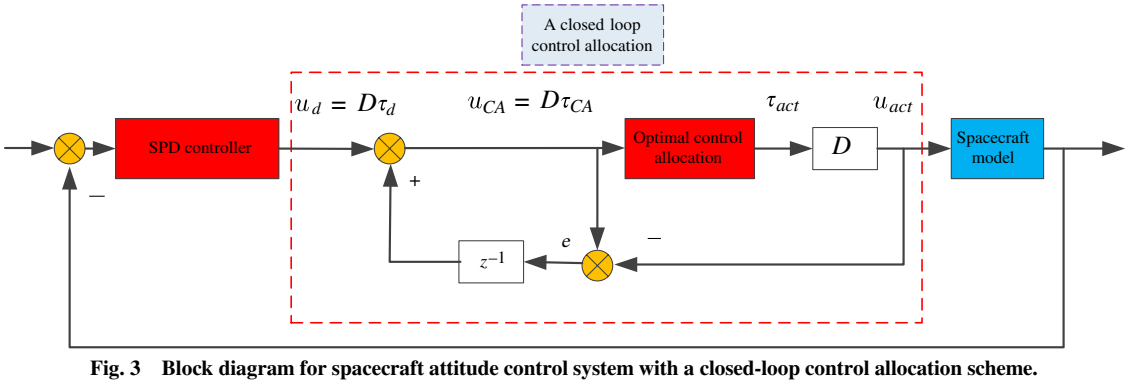

Fig. 3 Block diagram for spacecraft attitude control system with a closed-loop control allocation scheme.

where $\boldsymbol{DED}^{\dagger} = \boldsymbol{L}$. Then the eigenvalues of $\boldsymbol{L}$, defined as ℓ_i in the domain of (0,1), can be guaranteed. That is to say, the system (19) is asymptotically stable for a bounded virtual control command.

Proof: To analyze the stability of the closed-loop system including this presented closed-loop CA, the actual actuator torques can be described in a discrete-time model as follows:

$$\begin{aligned}\boldsymbol{\tau}_{\text{act}}(k) &= \boldsymbol{E}\boldsymbol{\tau}_{\text{CA}}(k) + \boldsymbol{F}\boldsymbol{\tau}_{\text{act}}(k-1) + \boldsymbol{G}\boldsymbol{u}_d(k) \\ &= \boldsymbol{E}\boldsymbol{D}^{\dagger}\boldsymbol{u}_{\text{CA}}(k) + \boldsymbol{F}\boldsymbol{\tau}_{\text{act}}(k-1) + \boldsymbol{G}\boldsymbol{u}_d(k)\end{aligned} \tag{20}$$

where

$$\boldsymbol{u}_{\text{CA}}(k) = \boldsymbol{u}_d(k) + \boldsymbol{e}(k-1) = \boldsymbol{u}_d(k) + \boldsymbol{u}_{\text{CA}}(k-1) - \boldsymbol{u}_{\text{act}}(k-1) \tag{21}$$

From Eqs. (20) and (21), one can obtain

$$\boldsymbol{u}_{\text{act}}(k) = \boldsymbol{D}\boldsymbol{\tau}_{\text{act}}(k) = \boldsymbol{D}\boldsymbol{E}\boldsymbol{D}^{\dagger}\boldsymbol{u}_{\text{CA}}(k) + \boldsymbol{D}\boldsymbol{F}\boldsymbol{\tau}_{\text{act}}(k-1) + \boldsymbol{D}\boldsymbol{G}\boldsymbol{u}_d(k) \tag{22}$$

$$\begin{aligned}\boldsymbol{D}\boldsymbol{E}\boldsymbol{D}^{\dagger}\boldsymbol{u}_{\text{CA}}(k) &= \boldsymbol{D}\boldsymbol{E}\boldsymbol{D}^{\dagger}\boldsymbol{u}_d(k) + \boldsymbol{D}\boldsymbol{E}\boldsymbol{D}^{\dagger}\boldsymbol{u}_{\text{CA}}(k-1) \\ &\quad - \boldsymbol{D}\boldsymbol{E}\boldsymbol{D}^{\dagger}\boldsymbol{u}_{\text{act}}(k-1)\end{aligned} \tag{23}$$

Subsequently, defining $\boldsymbol{DED}^{\dagger} = \boldsymbol{L}$ and substituting Eq. (22) to Eq. (23), one can obtain

$$\begin{aligned}\boldsymbol{L}\boldsymbol{u}_{\text{CA}}(k) &= \boldsymbol{L}\boldsymbol{u}_d(k) + \boldsymbol{u}_{\text{act}}(k-1) - \boldsymbol{D}\boldsymbol{F}\boldsymbol{\tau}_{\text{act}}(k-2) \\ &\quad - \boldsymbol{D}\boldsymbol{G}\boldsymbol{u}_d(k-1) - \boldsymbol{L}\boldsymbol{u}_{\text{act}}(k-1)\end{aligned} \tag{24}$$

and further with

$$\begin{aligned}\boldsymbol{u}_{\text{act}}(k) - (\boldsymbol{I}-\boldsymbol{L})\boldsymbol{u}_{\text{act}}(k-1) &= (\boldsymbol{L}+\boldsymbol{D}\boldsymbol{G})\boldsymbol{u}_d(k) - \boldsymbol{D}\boldsymbol{G}\boldsymbol{u}_d(k-1) \\ &\quad + \boldsymbol{D}\boldsymbol{F}(\boldsymbol{\tau}_{\text{act}}(k-1) - \boldsymbol{\tau}_{\text{act}}(k-2))\end{aligned} \tag{25}$$

Using the standard Z-transform theory, one can obtain the discrete-time model of the closed-loop control allocation system as follows:

$$\begin{aligned}\boldsymbol{U}_{\text{act}}(z) - z^{-1}(\boldsymbol{I}-\boldsymbol{L})\boldsymbol{U}_{\text{act}}(z) &= (\boldsymbol{L}+\boldsymbol{D}\boldsymbol{G})\boldsymbol{U}_d(z) - z^{-1}\boldsymbol{D}\boldsymbol{G}\boldsymbol{U}_d(z) \\ &\quad + \boldsymbol{D}\boldsymbol{F}(z^{-1}\boldsymbol{\Gamma}_{\text{act}}(z) - z^{-2}\boldsymbol{\Gamma}(z))\end{aligned}$$

that is,

$$\begin{aligned}(\boldsymbol{I} - z^{-1}(\boldsymbol{I}-\boldsymbol{L}))\boldsymbol{U}_{\text{act}}(z) &= (\boldsymbol{L}+\boldsymbol{D}\boldsymbol{G} - z^{-1}\boldsymbol{D}\boldsymbol{G})\boldsymbol{U}_d(z) \\ &\quad + \boldsymbol{D}\boldsymbol{F}z^{-1}(1-z^{-1})\boldsymbol{\Gamma}_{\text{act}}(z)\end{aligned}$$

Because the discrete-time model of the closed-loop control allocation system is obtained as in Eq. (19), the dynamic properties of the closed-loop system with the SPD baseline controller and closed-loop CA scheme ought to be studied subsequently. Then the characteristic equation of the closed-loop control allocation system from Eq. (19) can be obtained as follows [20,28]:

$$|\boldsymbol{I} - z^{-1}(\boldsymbol{I}-\boldsymbol{L})| = 0$$

that is,

$$|z\boldsymbol{I} - (\boldsymbol{I}-\boldsymbol{L})| = 0 \tag{26}$$

Based on the fundamental theorem of the discrete-time system, the necessary and sufficient condition for a discrete- time system to be stable is that the norms of all the characteristic roots are smaller than one [33]. Obviously, if the eigenvalues of $\boldsymbol{I}-\boldsymbol{L}$ defined as ς_i are in the domain of (0,1), that is to say, the eigenvalues of $\boldsymbol{L}$ defined as $\ell_i = 1 - \varsigma_i$ are in the domain of (0,1), then the closed-loop control allocation system described in Eq. (19) is stable. Based on similar rationale as proposed in [17,18,28,31], the overall closed-loop system is also stable because the SPD-based baseline controller has been designed to guarantee the stability of the attitude dynamic system of the spacecraft, although other types of controllers could also be used as the baseline controller, but without approved stability guarantee other than the SPD controller proposed and proved in this paper.

The eigenvalues of the characteristic equation of the closed-loop control allocation system can be obtained as follows:

$$\begin{aligned}\boldsymbol{L} = \boldsymbol{D}\boldsymbol{E}\boldsymbol{D}^{\dagger} &= \boldsymbol{D}(\boldsymbol{I}-\boldsymbol{G}\boldsymbol{D})\boldsymbol{W}^{-2}(\boldsymbol{R}_1\boldsymbol{W}_1)^2\boldsymbol{D}^{\dagger} \\ &= \boldsymbol{D}\boldsymbol{W}^{-1}(\boldsymbol{I} - (\boldsymbol{D}\boldsymbol{W}^{-1})^{\dagger}\boldsymbol{D}\boldsymbol{W}^{-1})\boldsymbol{W}^{-1}(\boldsymbol{R}_1\boldsymbol{W}_1)^2\boldsymbol{D}^{\dagger}\end{aligned} \tag{27}$$

Let the singular value decomposition of $\boldsymbol{D}$ and $\boldsymbol{DW}^{-1}$ be represented as

$$\boldsymbol{D} = \boldsymbol{U}_1\boldsymbol{\Sigma}_1\boldsymbol{V}_1^T = \boldsymbol{U}_1[\boldsymbol{\Sigma}_{1r} \quad 0]\begin{bmatrix}\boldsymbol{V}_{1r}^T \\ \boldsymbol{V}_{10}^T\end{bmatrix} = \boldsymbol{U}_1\boldsymbol{\Sigma}_{1r}\boldsymbol{V}_{1r}^T$$

$$\boldsymbol{D}\boldsymbol{W}^{-1} = \boldsymbol{U}_2\boldsymbol{\Sigma}_2\boldsymbol{V}_2^T = \boldsymbol{U}_2[\boldsymbol{\Sigma}_{2r} \quad 0]\begin{bmatrix}\boldsymbol{V}_{2r}^T \\ \boldsymbol{V}_{20}^T\end{bmatrix} = \boldsymbol{U}_2\boldsymbol{\Sigma}_{2r}\boldsymbol{V}_{2r}^T$$

where $\boldsymbol{U}_1$, $\boldsymbol{V}_1$, $\boldsymbol{U}_2$, and $\boldsymbol{V}_2$ are unitary matrixes, $\boldsymbol{\Sigma}_1$ and $\boldsymbol{\Sigma}_2$ are diagonal matrixes with strictly positive diagonal entries and their dimensions are equal to the rank of $\boldsymbol{D}$ and $\boldsymbol{DW}^{-1}$, respectively. Then these will yield

$$\boldsymbol{L} = \boldsymbol{U}_1\boldsymbol{\Sigma}_1\boldsymbol{V}_1^T\boldsymbol{W}^{-1}\boldsymbol{V}_{20}\boldsymbol{V}_{20}^T\boldsymbol{W}^{-1}(\boldsymbol{R}_1\boldsymbol{W}_1)^2\boldsymbol{V}_1\boldsymbol{\Sigma}_1^{-1}\boldsymbol{U}_1^T$$

Using the basic results and techniques of matrix theory [34], the nonzero eigenvalues of matrix product $\boldsymbol{MN}$, the following equation can be obtained:

$$\ell_{nz}(\boldsymbol{M}\boldsymbol{N}) = \ell_{nz}(\boldsymbol{N}\boldsymbol{M})$$

where ℓ_{nz} denotes the nonzero eigenvalues of the matrix.

From the preceding analysis, one can further obtain that

$$\begin{aligned}\ell_{nz}(\boldsymbol{L}) &= \ell_{nz}(\boldsymbol{V}_{20}^T\boldsymbol{W}^{-1}(\boldsymbol{R}_1\boldsymbol{W}_1)^2\boldsymbol{V}_1\boldsymbol{\Sigma}_1^{-1}\boldsymbol{U}_1^T\boldsymbol{U}_1\boldsymbol{\Sigma}_1\boldsymbol{V}_1^T\boldsymbol{W}^{-1}\boldsymbol{V}_{20}) \\ &= \ell_{nz}(\boldsymbol{V}_{20}^T\boldsymbol{W}^{-1}(\boldsymbol{R}_1\boldsymbol{W}_1)^2\boldsymbol{W}^{-1}\boldsymbol{V}_{20})\end{aligned}$$

Next, the following result can be achieved from the definition of matrix singular values

$$\ell_{nz}(\boldsymbol{V}_{20}^T\boldsymbol{W}^{-1}(\boldsymbol{R}_1\boldsymbol{W}_1)^2\boldsymbol{W}^{-1}\boldsymbol{V}_{20}) = \sigma^2(\boldsymbol{R}_1\boldsymbol{W}_1\boldsymbol{W}^{-1}\boldsymbol{V}_{20}) > 0 \tag{28}$$

which states that the nonzero eigenvalues of $\boldsymbol{L}$ are real and positive. That is, $\ell_{nz}(\boldsymbol{L}) > 0$ can be guaranteed.

On the other hand, what remains to be shown is that the eigenvalues of $\boldsymbol{L}$ are bounded by one, and let the maximum eigenvalue of $\boldsymbol{L}$ be $\ell_{\max}(\boldsymbol{L})$, namely,

$$\begin{aligned}\ell_{\max}(\boldsymbol{L}) = \sigma_{\max}^2(\boldsymbol{R}_1\boldsymbol{W}_1\boldsymbol{W}^{-1}\boldsymbol{V}_{20}) &= \|\boldsymbol{R}_1\boldsymbol{W}_1\boldsymbol{W}^{-1}\boldsymbol{V}_{20}\|^2 \\ &\le \|\boldsymbol{R}_1\boldsymbol{W}_1\boldsymbol{W}^{-1}\|^2\|\boldsymbol{V}_{20}\|^2 \le \|\boldsymbol{R}_1\boldsymbol{W}_1\boldsymbol{W}^{-1}\|^2\end{aligned}$$

which, using the property of singular value decomposition, that is, $\|\boldsymbol{V}_{20}\|^2 = \ell_{\max}(\boldsymbol{V}_{20}^T\boldsymbol{V}_{20}) = 1$. Then,

$$\ell_{\max}(\boldsymbol{L}) \le \|\boldsymbol{R}_1\boldsymbol{W}_1\boldsymbol{W}^{-1}\|^2 = \sup_{x\neq 0}\frac{\boldsymbol{x}^T\boldsymbol{W}^{-1}(\boldsymbol{R}_1\boldsymbol{W}_1)^2\boldsymbol{W}^{-1}\boldsymbol{x}}{\boldsymbol{x}^T\boldsymbol{x}} \tag{29}$$

Defining $\boldsymbol{W}^{-1}\boldsymbol{x} = \boldsymbol{y}$, then $\boldsymbol{W}\boldsymbol{y} = \boldsymbol{x}$, and so Eq. (29) can be redescribed as

$$\ell_{\max}(\boldsymbol{L}) \le \sup_{\boldsymbol{y}\neq 0} \frac{\boldsymbol{y}^T(\boldsymbol{R}_1\boldsymbol{W}_1)^2\boldsymbol{y}}{\boldsymbol{y}^T\boldsymbol{W}^2\boldsymbol{y}}$$
$$= \sup_{\boldsymbol{y}\neq 0} \frac{\boldsymbol{y}^T(\boldsymbol{R}_1\boldsymbol{W}_1)^2\boldsymbol{y}}{\boldsymbol{y}^T((\boldsymbol{R}_0\boldsymbol{W}_0)^2 + (\boldsymbol{R}_1\boldsymbol{W}_1)^2 + (\boldsymbol{W}_2)^2)\boldsymbol{y}}$$
$$\le \sup_{\boldsymbol{y}\neq 0} \frac{\boldsymbol{y}^T(\boldsymbol{R}_1\boldsymbol{W}_1)^2\boldsymbol{y}}{\boldsymbol{y}^T(\boldsymbol{R}_1\boldsymbol{W}_1)^2\boldsymbol{y}} = 1 \tag{30}$$

because $\boldsymbol{W}_0$, $\boldsymbol{W}_1$, and $\boldsymbol{W}_2$ denote the diagonal positive-defined weighting matrices, so that $\boldsymbol{y}^T((\boldsymbol{R}_0\boldsymbol{W}_0)^2 + (\boldsymbol{W}_2)^2)\boldsymbol{y} > 0$ for any $\boldsymbol{y} \neq 0$. From Eqs. (28) and (30), the eigenvalues of $\boldsymbol{L}$, defined as ℓ_i in the domain of (0,1), can be achieved. That is to say, the system (19) is asymptotically stable.

Remark 3: From the preceding stability analysis, one can see that the discrete-time method was used for the closed-loop control allocation system. On the one hand, the operating and working signals from the computer are discrete time in a practical engineering environment such as the orbiting spacecraft. On the other hand, it is also convenient for stability analysis and guarantee of the considered CA. In view of the whole process of the CA in Sec. III.B, the discrete-time analysis was useful and frequently used because of the special formulation of the proposed control allocation algorithm formulated as a constrained optimal quadratic programming problem as described in Eq. (15), so use of the standard Z-transform theory for the stability analysis is necessary and reasonable.

Remark 4: The formal proof of the overall closed-loop stability of the system (such as SPD + CA) still does not exist in the literature due to the special feature and difficulty of such a two-step or two-part control configuration. The proposed control scheme (SPD + CLCA) in this paper provides a reasonable solution to this problem and is the motivation and also the main contribution of the research results presented in this paper for such a difficult problem. In other words, most of the existing control allocation schemes are studied and worked as an open-loop system in some sense, and the stability/stabilization issue of a closed-loop system under combination of control allocation with the baseline controller is not considered due to the inherent difficulty for such a control design task. From this point of view, the developed control scheme in this paper is novel and has a significant contribution toward such a practical engineering application for spacecraft attitude control systems and also other overactuated systems.

IV. Simulation and Analysis

To verify the effectiveness and performance of the proposed attitude stabilization control and the closed-loop constrained optimal control allocation scheme, numerical simulations have been carried out using the rigid spacecraft system given in Eqs. (1) and (4). It should be noted that, for orbiting spacecraft, there are more than three actuators aligned with the three body-fixed axes of the spacecraft, therefore, a typical application case with an overactuated dynamic system. A common configuration with four reaction wheels is shown in Fig. 4 and is chosen as the spacecraft actuators in this paper. In such a configuration, the rotational axes of three reaction wheels (such as reaction wheels 1, 2, and 3) are orthogonal to the spacecraft's orthogonal shaft and the fourth one is installed with the equiangular direction with the orthogonal-to-each-other three axes.

However, in practice, the orthogonal configuration of actuators will never be perfect. Whether due to limited manufacturing tolerances or warping of the spacecraft structure during launch, some alignment errors can always exist. Referring to Fig. 5 and to model such uncertainties, it is assumed that the reaction wheel mounted on the x axis is tilted over nominal direction with constant angles $\Delta\alpha_1$ and $\Delta\beta_1$; also, other reaction wheels mounted left are assumed to be tilted over nominal direction with $\Delta\alpha_2$, $\Delta\beta_2$, $\Delta\alpha_3$, $\Delta\beta_3$, $\Delta\alpha_4$, and $\Delta\beta_4$, respectively.

To this end, the real reaction wheel torques with misalignments can be expressed as

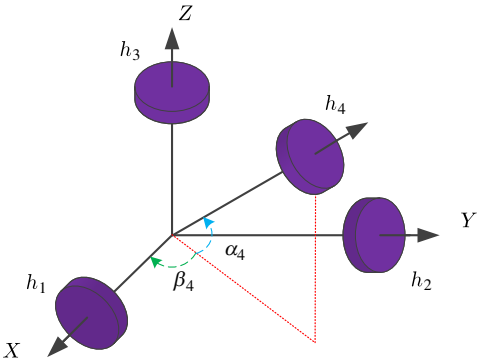

Fig. 4 Configuration of four reaction wheels in a spacecraft.

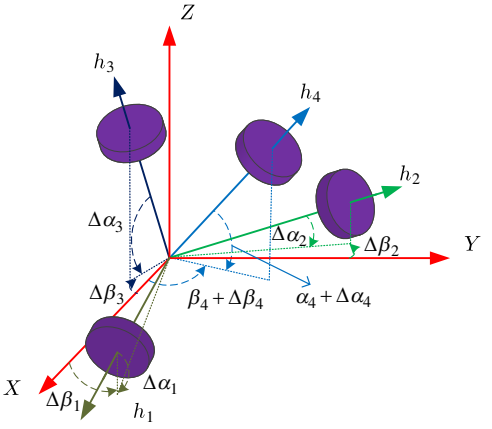

Fig. 5 Four reaction wheels with misalignment consideration.

$$u = \tau_1 \begin{bmatrix} \cos\Delta\alpha_1 \\ \sin\Delta\alpha_1\cos\Delta\beta_1 \\ \sin\Delta\alpha_1\sin\Delta\beta_1 \end{bmatrix} + \tau_2 \begin{bmatrix} \sin\Delta\alpha_2\cos\Delta\beta_2 \\ \cos\Delta\alpha_2 \\ \sin\Delta\alpha_2\sin\Delta\beta_2 \end{bmatrix}$$
$$+ \tau_3 \begin{bmatrix} \sin\Delta\alpha_3\cos\Delta\beta_3 \\ \sin\Delta\alpha_3\sin\Delta\beta_3 \\ \cos\Delta\alpha_3 \end{bmatrix} + \tau_4 \begin{bmatrix} \cos(\alpha_4+\Delta\alpha_4)\cos(\beta_4+\Delta\beta_4) \\ \cos(\alpha_4+\Delta\alpha_4)\sin(\beta_4+\Delta\beta_4) \\ \sin(\alpha_4+\Delta\alpha_4) \end{bmatrix}$$

Table 1 Main parameters of a rigid spacecraft

Mission	Attitude stabilization
Mass, kg	874.56
Inertia moments, kg·m^2	
Principal moments of inertia	$J_1 = 20, J_2 = 17, J_3 = 15$
Products of inertia	$J_{12} = 0, J_{23} = 0, J_{13} = 0.9$
Orbit	
Type	Circular
Attitude, km	500
Inclination, deg	97.4
Right ascension of the ascending node	1030 hrs
Attitude	
Attitude control type	Three-axis control by four reaction fly wheels
Initial attitude quaternion	$\boldsymbol{Q}_0 = [q_0, q^T]^T = [0.9; -0.3; 0.26; 0.18]$
Initial angular velocity, rad/s	$\boldsymbol{w}_0 = [0.1; -0.1; -0.05]$
Reaction fly wheels	
Maximum torque, N·m	0.5
Assembling locations/ angles, deg	$\alpha_4 = 35.26, \beta_4 = 45$
Misalignment error angles, deg	$\Delta\boldsymbol{\alpha} = [15; 10; 15; 10]$, $\Delta\boldsymbol{\beta} = [15; 10; 15; 10]$

Table 2 Control parameters chosen for numerical analysis

Control schemes	Control gains
SPD controller	$u_{\max} = 1, \beta = 0.908, \alpha^2 = 0.1$
Closed-loop control allocator	$\tau_{\min} = -0.5, \tau_{\max} = 0.5,$ $\eta_{\min} = -0.002, \eta_{\max} = 0.002,$ $\boldsymbol{W}_0 = \text{diag}(10 \quad 22 \quad 0.1 \quad 1),$ $\boldsymbol{W}_1 = \text{diag}(10 \quad 12 \quad 1 \quad 0.1),$ $\boldsymbol{W}_2 = \text{diag}(10 \quad 12 \quad 1 \quad 0.1)$
PD controller	$k_P = 6.2, k_D = 6.6$

Generally, the misalignment angle errors $(\Delta\alpha_i, \Delta\beta_i)$ are very small in practice, and the following relationships are adopted to approximate the operator for the preceding equation: $\cos\Delta\alpha_i \approx \cos\Delta\beta_i \approx 1$, $\sin\Delta\alpha_i \approx \Delta\alpha_i$, $\sin\Delta\beta_i \approx \Delta\beta_i$. Then, for the considered actuator configuration, the configuration matrix $\boldsymbol{D}$ in Eq. (7b) can be represented as

$$\boldsymbol{D} = \boldsymbol{D}_0 + \Delta\boldsymbol{D} \tag{31}$$

with

$$\boldsymbol{D}_0 = \begin{bmatrix} 1 & 0 & 0 & \cos\alpha_4\cos\beta_4 \\ 0 & 1 & 0 & \cos\alpha_4\sin\beta_4 \\ 0 & 0 & 1 & \sin\alpha_4 \end{bmatrix} \tag{32a}$$

where $\boldsymbol{D}_0$ denotes the nominal value of the distribution matrix of over-actuated actuators, and $\Delta\boldsymbol{D}$ denotes the uncertainty of the distribution matrix. The external disturbances are assumed to be as follows:

$$\boldsymbol{d}(t) = 0.2\times10^{-3}\begin{bmatrix} 3\cos(10\omega_d t) + 4\sin(3\omega_d t) - 10 \\ -1.5\sin(2\omega_d t) + 3\cos(5\omega_d t) + 15 \\ 3\sin(10\omega_d t) - 8\sin(4\omega_d t) + 10 \end{bmatrix}\text{N.m}$$

For comparison purposes, the widely used PD controller [10] and also the PI control allocation [18] are applied to the problem considered. Note that PI is a kind of open-loop control allocation scheme. More specifically, simulations using the following four control schemes are conducted: case 1, the PD controller incorporating the PI control allocator, noted as PD + PI; case 2, the proposed SPD controller combined with the PI control allocator, noted as SPD + PI; case 3, the proposed SPD controller incorporating the proposed CLCA, noted as SPD + CLCA; and case 4, the PD controller incorporating the proposed CLCA scheme, noted as PD + CLCA.

More specially, performances of the attitude stabilization control system with/without actuator uncertainties and external disturbances are discussed, respectively, in the preceding different cases, and the simulation parameters are provided in Tables 1 and 2 for all numerical simulations carried out in the MATLAB/Simulink software environment; the sampling time for all the simulations is $T_s = 0.2$ s.

A. Attitude Control Without Actuator Uncertainties and Disturbances

In this simulation case, the proposed control scheme SPD + CLCA is first applied to the rigid spacecraft attitude stabilization control system. Further, the SPD and PD + PI schemes are studied for the purpose of comparison. Figures 6 and 7 show the time

$$\Delta\boldsymbol{D} = \begin{bmatrix} 0 & \Delta\alpha_2\cos\Delta\beta_2 & \Delta\alpha_3\cos\Delta\beta_3 & -\Delta\alpha_4\sin\alpha_4\cos\beta_4 - \Delta\beta_4\cos\alpha_4\sin\beta_4 \\ \Delta\alpha_1\cos\Delta\beta_1 & 0 & \Delta\alpha_3\sin\Delta\beta_3 & -\Delta\alpha_4\sin\alpha_4\sin\beta_4 + \Delta\beta_4\cos\alpha_4\cos\beta_4 \\ \Delta\alpha_1\sin\Delta\beta_1 & \Delta\alpha_2\sin\Delta\beta_2 & 0 & \Delta\alpha_4\cos\alpha_4 \end{bmatrix} \tag{32b}$$

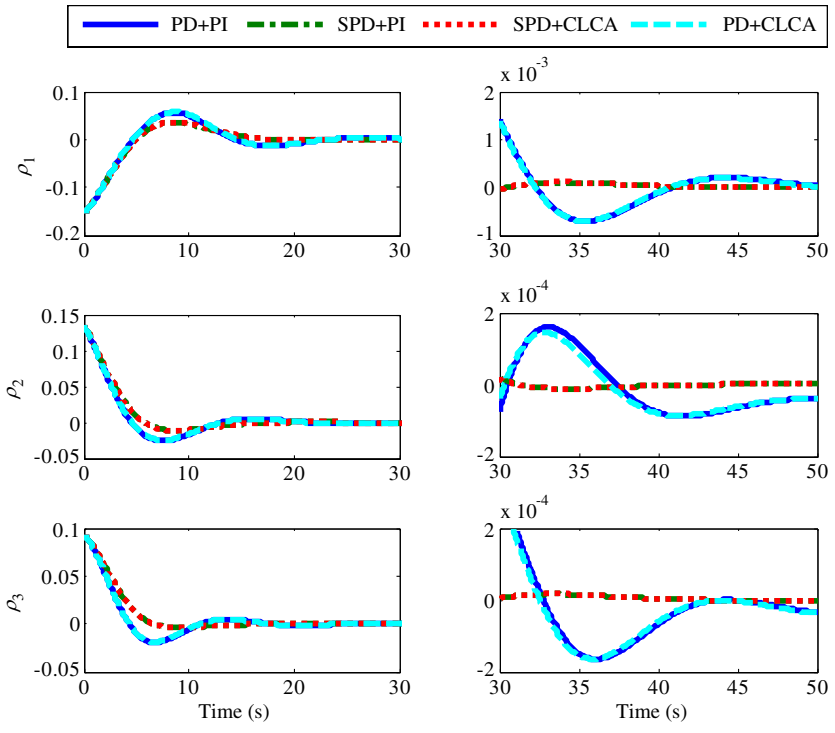

Fig. 6 Time responses of the spacecraft attitude MRPs ρ.

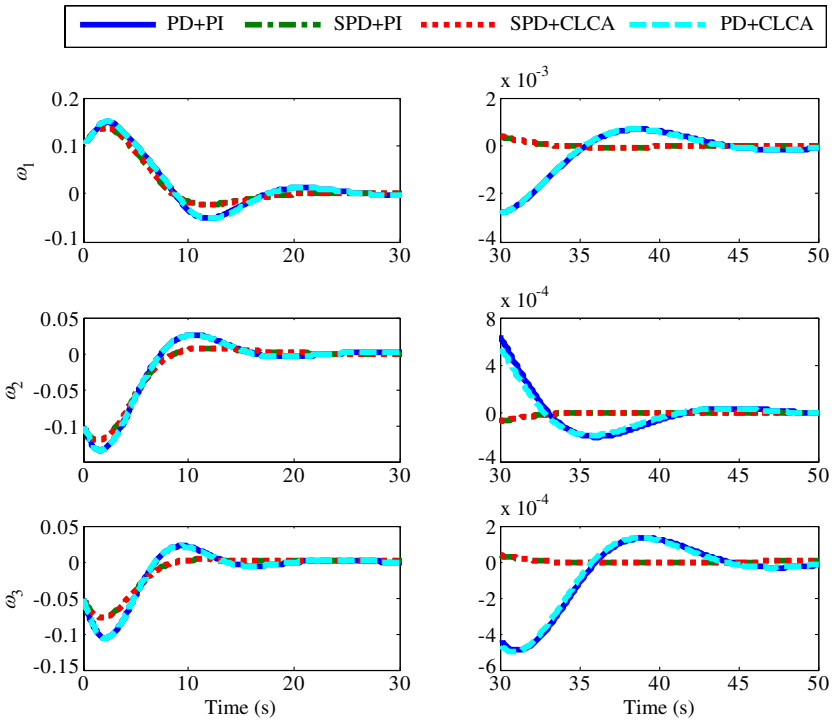

Fig. 7 Time responses of the spacecraft attitude angular velocity ω.

responses of the attitude MRPs and angular velocity, respectively, under the case of without actuator uncertainties and external disturbances. As it can be seen, the SPD + CLCA (dotted line) could achieve the best performance among them. The spacecraft attitude system reaches the commanded target smoothly with a settling time less than 20 s and a high accuracy of 10–4 in steady-state error. The SPD + PI (dashed-dotted line) achieves a similar response as the SPD + CLCA because they are worked in such an ideal (without uncertainty and disturbance) and normal mode. However, a longer settling time with more than 30 s and transient response with oscillations are observed with the PD + PI (solid line) and PD + CLCA (dashed line) schemes. Despite the fact that there may exist further room for improvement with better tuning of the control parameters, there is not much improvement in the attitude responses with PD + PI and PD + CLCA schemes due to the limitation of the baseline controller PD. The time response of demanded/virtual control torques and the actual actuator/reaction flywheel torques are shown in Figs. 8 and 9, respectively. Note that the restriction on the actuator output torque magnitude 0.5 N·m is considered explicitly. Thanks to the designed SPD controller and the closed-loop constrained optimal control allocator, the specified actuator constraints have been met by the SPD + CLCA. However, the other schemes

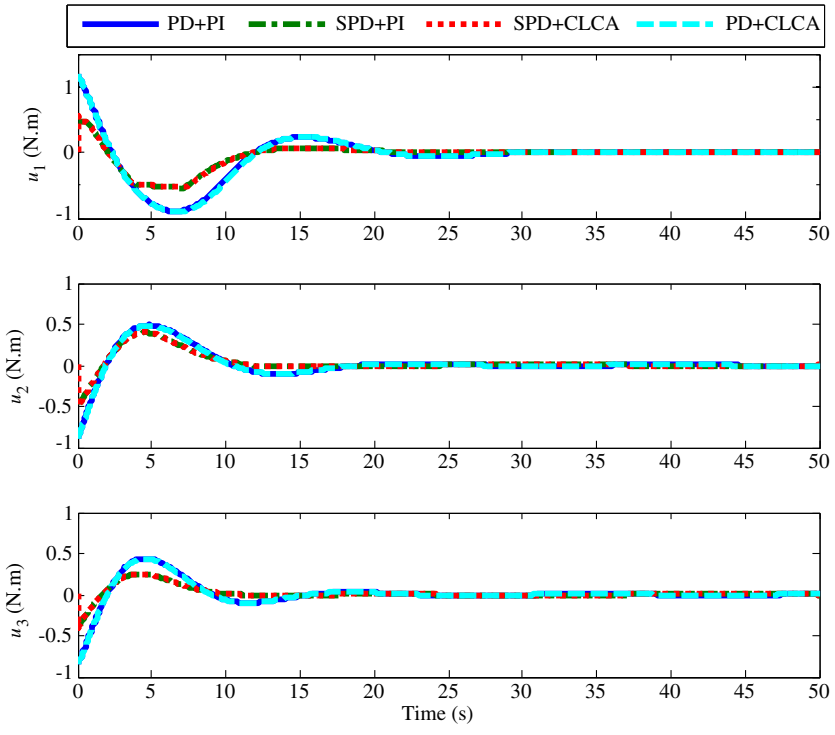

Fig. 8 Time responses of the demanded/virtual control torques u.

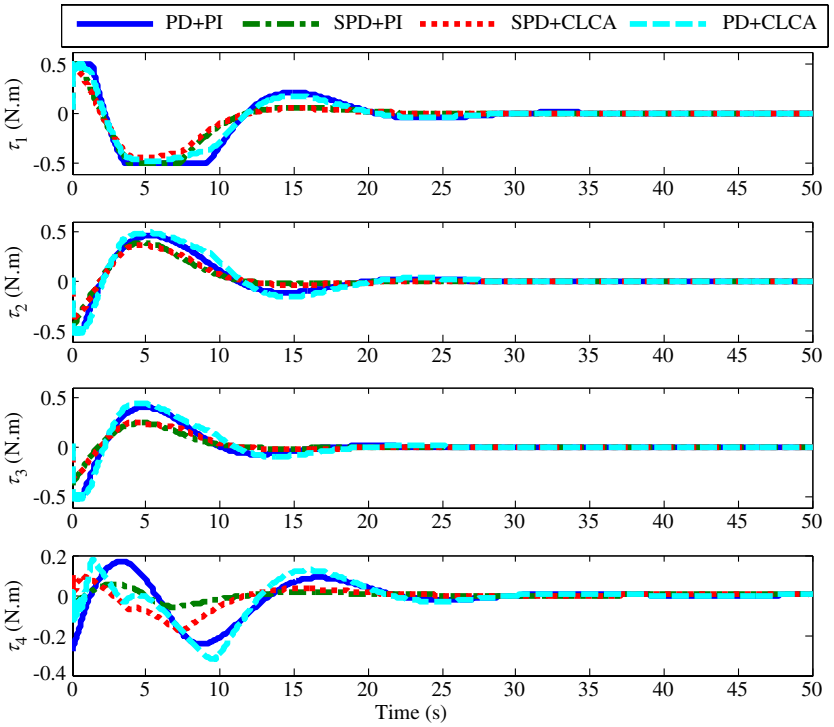

Fig. 9 Time responses of the actual actuator control torques τ.

achieve relatively worse performance with respect to actuator constraints, especially for PD + PI. As shown in Fig. 8, comparing the cases among SPD + CLCA, PD + CLCA, and PD + PI, the control signals (u_1, u_2, u_3) of the PD controller are obviously larger than those with the SPD controller, whereas the PD + PI scheme leads also to the saturated reaction wheel torque in τ_1 with a longer period. Comparing the responses between SPD + CLCA and PD + CLCA, improved performance has been achieved, which shows the necessity and better performance of the proposed SPD controller over the conventional PD controller.

Time responses of the closed-loop control allocation errors are shown in Fig. 10. It shows clearly that the errors of the closed-loop control allocation converge to zero within 20 s and further expounds and proves the stability of the closed-loop control allocation system. Additionally, fuel or electrical energy saving for spacecraft in orbit is of crucial importance to prolong the working life and to achieve the targeted missions. Therefore, the energy consumption optimization problem should also be considered for the spacecraft attitude control system. To analyze the system energy consumption, the performance function that is derived from the optimal control allocation problem is defined as

$$\mathbf{E} = \frac{1}{2}\int_0^T \|\boldsymbol{\tau}\|^2 \, \mathrm{d}t$$

where T denotes the simulation time, and $T = 50$ s is chosen in the simulation. Figure 11 shows the bar graphic visualizations of the energy consumption performance among the four control strategies without actuator uncertainties and external disturbances. From Fig. 11, it can be seen clearly that the energy consumption using SPD + CLCA presented in this paper is relatively minimal in the four settling intervals, although more energy is consumed to achieve the desired targets because there is no energy optimization constraint in the traditional controller PD with control allocator PI. Results of SPD + PI/PD + PI are close to those of SPD + CLCA/PD + CLCA, but still required higher energy consumption than the latter one.

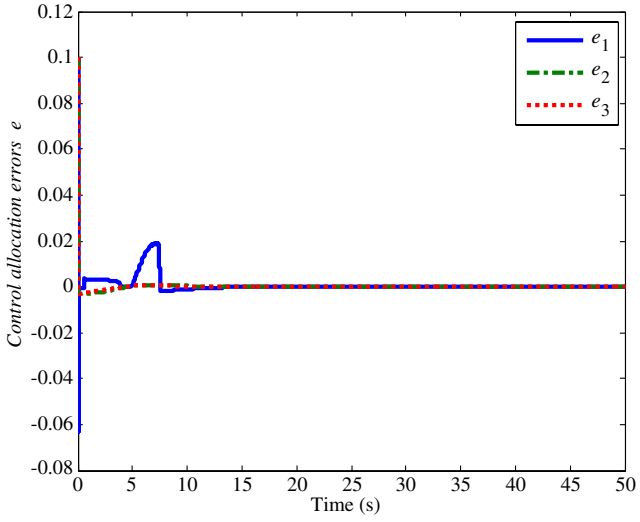

Fig. 10 Time responses of the closed-loop control allocation errors.

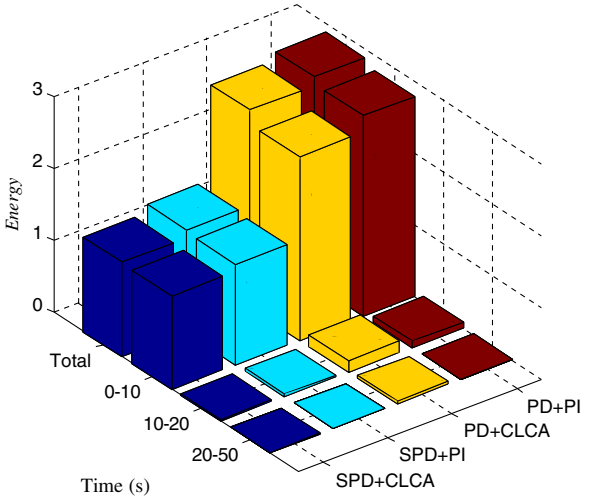

Fig. 11 Bar graphic visualizations of the energy consumption performance comparisons of four schemes.

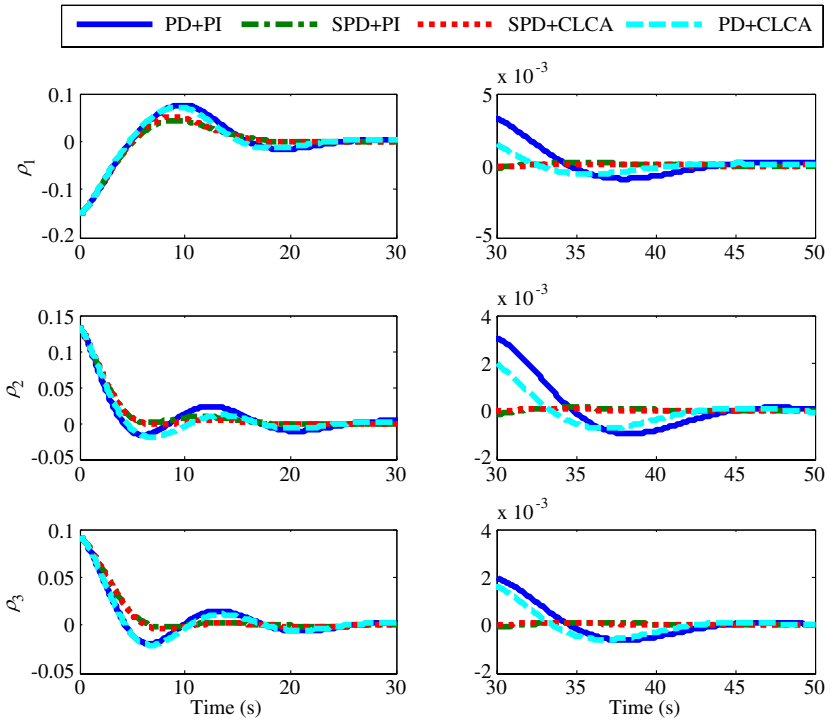

Fig. 12 Time responses of the spacecraft attitude MRPs ρ.

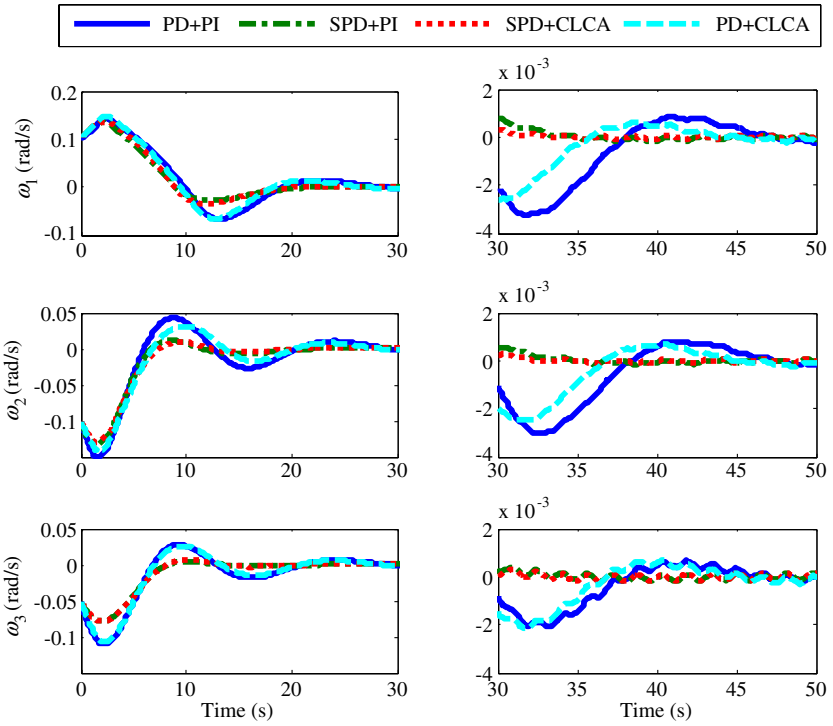

Fig. 13 Time responses of the spacecraft attitude angular velocity ω.

B. Attitude Control with Actuator Uncertainties and Disturbances

Actuator uncertainties and external disturbances are considered for the rigid spacecraft attitude stabilization control system in this subsection and results are presented subsequently. First, Figs. 12 and 13 represent time responses of the attitude MRPs and angular velocities, respectively. As can be observed, the SPD + CLCA (dotted line) and SPD + PI (dashed-dotted line) achieve good and similar performance. The spacecraft attitude system reaches the commanded stabilization target smoothly with a settling time less than 25 s with a high accuracy in steady-state error. However, a longer settling time (more than 30 s) and a lower accuracy can be observed in the PD + PI (solid line) and PD + CLCA (dashed line) schemes, which demonstrates further the improved performance of the proposed SPD controller as shown in Sec. IV.A. The time response of the demanded/virtual control torques and the actual actuator/reaction flywheel torques are shown in Figs. 14 and 15, respectively. Although the SPD + PI scheme achieves a similar performance in spacecraft attitude state compared with the SPD + CLCA scheme, it sacrifices more torque/energy to achieve it, which is a less preferable action in the practical deep-space mission for spacecraft compared with the

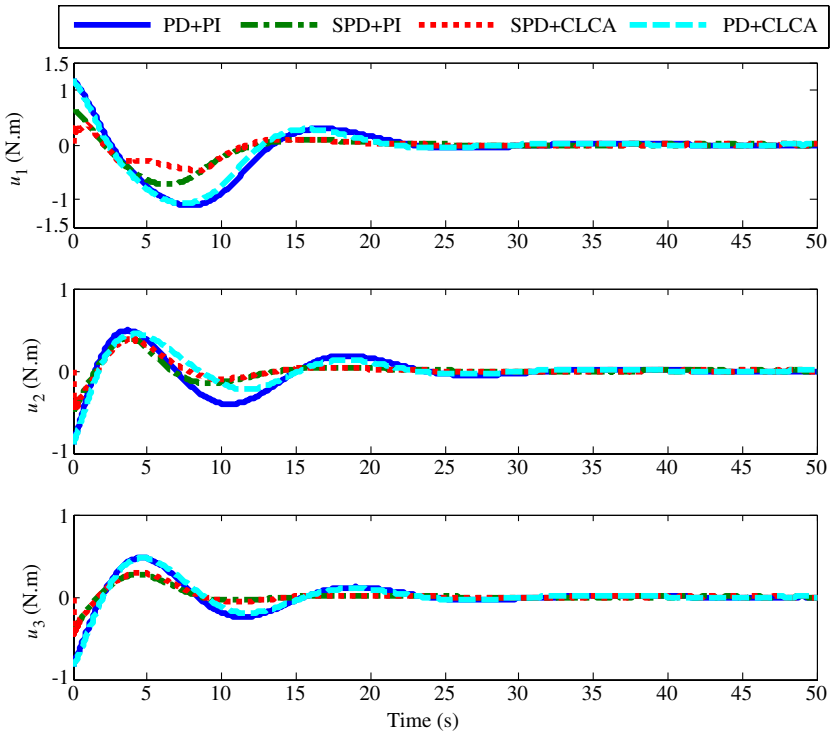

Fig. 14 Time responses of the demanded/virtual control torques u.

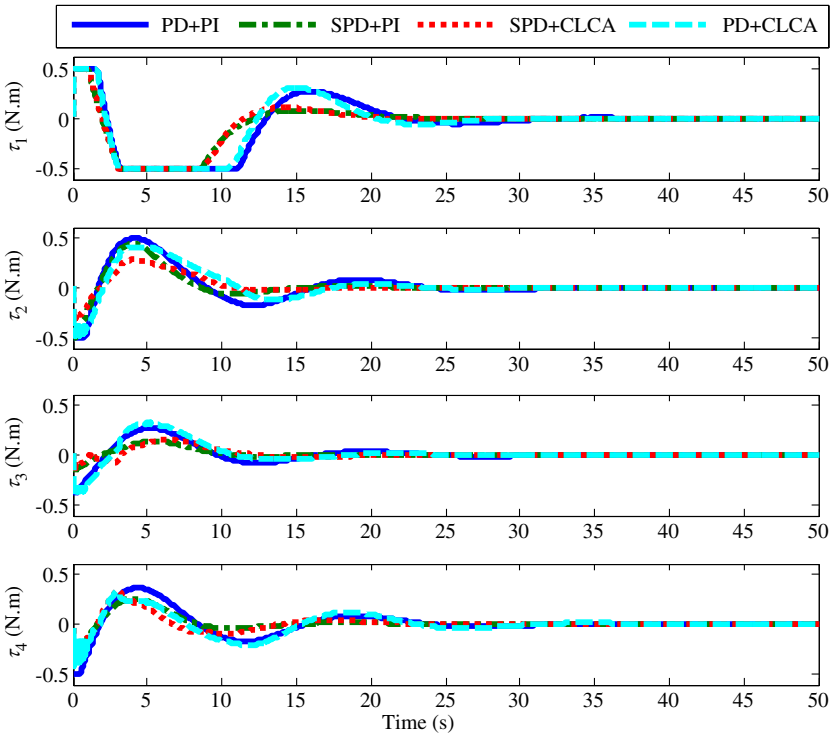

Fig. 15 Time responses of the actual actuator control torques τ.

SPD + CLCA scheme that also provides a stability guarantee as proved in Sec. III.B.2, and is shown in Fig. 16 for the time responses of the closed-loop control allocation errors. In addition, the bar graphic visualizations of the energy consumption performance among the four control strategies with actuator uncertainties and external disturbances are shown in Fig. 17, and it can be seen clearly that the energy consumption of the SPD + CLCA presented in this paper is minimum and an obvious improvement over SPD + PI has been achieved compared with the case without actuator uncertainties and external disturbances. Such an improvement is benefitted and achieved by the closed-loop constrained optimal control allocator proposed in this paper and it is more robust to uncertainties and disturbances and more suitable to meet the practical requirements for orbiting spacecraft.

Summarizing all the control schemes and test scenarios presented previously, the proposed control scheme SPD + CLCA can improve the normal performance more significantly than the other two methods, whether the actuator uncertainties and external disturbances are

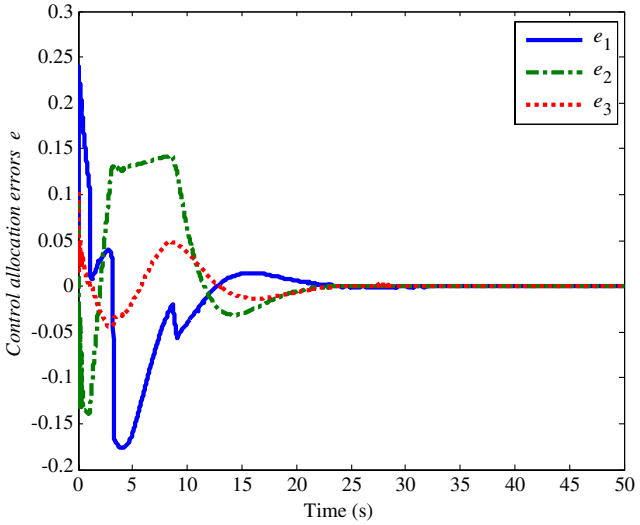

Fig. 16 Time responses of the closed-loop control allocation errors.

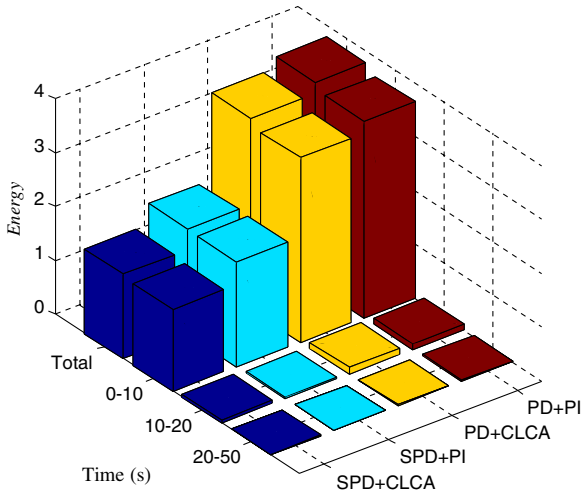

Fig. 17 Bar graphic visualizations of the energy consumption performance comparisons of four cases.

considered or not. Most significantly, the proposed SPD + CLCA can be proved theoretically for ensuring the system to be stable with a specified trajectory. Extensive simulations were also carried out using different control parameters and disturbances. These results show that, in the closed-loop system, attitude stabilization control and energy saving have been accomplished in spite of these undesired uncertainties in the system. Moreover, the flexibility in the choice of controller and control allocator parameters can be used to obtain a desirable performance while meeting the position and rate constraints of the actuators. These control approaches provide the theoretical foundations for the practical application of the advanced control theory to spacecraft attitude control systems design.

V. Conclusions

In this paper, a saturated proportional-derivative nonlinear control strategy has been incorporated into a novel closed-loop constrained optimal control allocation framework to solve the attitude stabilization control problem of a rigid spacecraft. Specifically, a saturated proportional-derivative nonlinear control law is first designed as the baseline/virtual feedback controller to achieve attitude stabilization explicitly, considering control input/signal constraints with respect to actuator saturation limits. Then, a closed-loop constrained optimal control allocation scheme is further developed by considering the actuator position and rate constraints simultaneously to suitably distribute the virtual control command determined by the baseline controller into the redundant actuators. Furthermore, the asymptotical stability of the closed-loop system has been proved and guaranteed. Finally, numerical simulations of the proposed novel control strategy were also presented to demonstrate the advantages and improvements with respect to the time responses and energy consumption saving over existing methods, especially by taking into account the actuator uncertainties and external disturbances as well. It should be pointed out that actuator faults such as loss of effectiveness or stuck are not considered directly in this paper, which is one of the subjects for our future research.

Acknowledgments

Financial support of this work by the National Natural Science Foundation of China (Project 61004072, 61273175), Program for New Century Excellent Talents in University (NCET-11-0801), Heilongjiang Province Science Foundation for Youths (QC2012C024), as well as Natural Sciences and Engineering Research Council of Canada through a Strategic Project Grant and a Discovery Project Grant are highly acknowledged. The authors would like to thank Narendra Gollu, Sean Zhang, the reviewers, and the editor for their comments and suggestions that helped to improve the paper significantly.

References

[1] Krstic, M., and Tsiotras, P., "Inverse Optimal Stabilization of a Rigid Spacecraft," *IEEE Transactions on Automatic Control*, Vol. 44, No. 5, 1999, pp. 1042–1049. doi:10.1109/9.763225

[2] Xing, G. Q., and Parvez, S. A., "Nonlinear Attitude State Tracking Control for Spacecraft," *Journal of Guidance, Control, and Dynamics*, Vol. 24, No. 3, 2001, pp. 624–626. doi:10.2514/2.4754

[3] Wie, B., and Lu, J. B., "Feedback-Control Logic for Spacecraft Eigenaxis Rotations Under Slew Rate and Control Constraints," *Journal of Guidance, Control, and Dynamics*, Vol. 18, No. 6, 1995, pp. 1372–1379. doi:10.2514/3.21555

[4] Junkins, J. L., Akella, M. R., and Robinett, R. D., "Nonlinear Adaptive Control of Spacecraft Maneuvers," *Journal of Guidance, Control, and Dynamics*, Vol. 20, No. 6, 1997, pp. 1104–1110. doi:10.2514/2.4192

[5] Joshi, S. M., Kelkar, A. G., and Wen, J. T. Y., "Robust Attitude Stabilization of Spacecraft Using Nonlinear Quaternion Feedback," *IEEE Transactions on Automatic Control*, Vol. 40, No. 10, 1995, pp. 1800–1803. doi:10.1109/9.467669

[6] Boskovic, J. D., Li, S. M., and Mehra, R. K., "Robust Tracking Control Design for Spacecraft Under Control Input Saturation," *Journal of Guidance, Control, and Dynamics*, Vol. 27, No. 4, 2004, pp. 627–633. doi:10.2514/1.1059

[7] Hu, Q. L., "Robust Adaptive Sliding Mode Attitude Maneuvering and Vibration Damping of Three-Axis-Stabilized Flexible Spacecraft with Actuator Saturation Limits," *Nonlinear Dynamics*, Vol. 55, No. 4, 2009, pp. 301–321. doi:10.1007/s11071-008-9363-1

[8] Tsiotras, P., "Further Passivity Results for the Attitude Control Problem," *IEEE Transactions on Automatic Control*, Vol. 43, No. 11, 1998, pp. 1597–1600. doi:10.1109/9.728877

[9] Tsiotras, P., "Stabilization and Optimality Results for the Attitude Control Problem," *Journal of Guidance, Control, and Dynamics*, Vol. 19, No. 4, 1996, pp. 772–779. doi:10.2514/3.21698

[10] Wen, J. T. Y., and Kreutzdelgado, K., "The Attitude-Control Problem," *IEEE Transactions on Automatic Control*, Vol. 36, No. 10, 1991, pp. 1148–1162. doi:10.1109/9.90228

[11] Slotine, J. J. E., and Li, W., *Applied Nonlinear Control*, Prentice–Hall, Englewood Cliffs, NJ, 1991, pp. 72–73.

[12] Xiao, B., Hu, Q. L., and Zhang, Y. M., "Angular Velocity-Free Control for Rigid Spacecraft Attitude Stabilization Under Input Constraint," *18th IFAC World Congress*, Elsevier, New York, 2011, pp. 8491–8496.

[13] Ali, I., Radice, G., and Kim, J., "Backstepping Control Design with Actuator Torque Bound for Spacecraft Attitude Maneuver," *Journal of Guidance, Control, and Dynamics*, Vol. 33, No. 1, 2010, pp. 254–259. doi:10.2514/1.45541

[14] Boskovic, J. D., Li, S. M., and Mehra, R. K., "Robust Adaptive Variable Structure Control of Spacecraft Under Control Input Saturation," *Journal of Guidance, Control, and Dynamics*, Vol. 24, No. 1, 2001, pp. 14–22. doi:10.2514/2.4704

[15] Su, Y. X., and Zheng, C. H., "Globally Asymptotic Stabilization of Spacecraft with Simple Saturated Proportional-Derivative Control," *Journal of Guidance, Control, and Dynamics*, Vol. 34, No. 6, 2011, pp. 1932–1936. doi:10.2514/1.54254

[16] Wallsgrove, R. J., and Akella, M. R., "Globally Stabilizing Saturated Attitude Control in the Presence of Bounded Unknown Disturbances," *Journal of Guidance, Control, and Dynamics*, Vol. 28, No. 5, 2005, pp. 957–963. doi:10.2514/1.9980

[17] Buffington, J. M., and Enns, D. F., "Lyapunov Stability Analysis of Daisy Chain Control Allocation," *Journal of Guidance, Control, and Dynamics*, Vol. 19, No. 6, 1996, pp. 1226–1230. doi:10.2514/3.21776

[18] Buffington, J. M., Enns, D. F., and Teel, A. R., "Control Allocation and Zero Dynamics," *Journal of Guidance, Control, and Dynamics*, Vol. 21, No. 3, 1998, pp. 458–464. doi:10.2514/2.4258

[19] Durham, W. C., "Constrained Control Allocation," *Journal of Guidance, Control, and Dynamics*, Vol. 16, No. 4, 1993, pp. 717–725. doi:10.2514/3.21072

[20] Harkegard, O., "Dynamic Control Allocation Using Constrained Quadratic Programming," *Journal of Guidance, Control, and Dynamics*, Vol. 27, No. 6, 2004, pp. 1028–1034. doi:10.2514/1.11607

[21] Harkegard, O., and Glad, S. T., "Resolving Actuator Redundancy—Optimal Control vs. Control Allocation," *Automatica*, Vol. 41, No. 1, 2005, pp. 137–144. doi:10.1016/j.automatica.2004.09.007

[22] Shi, Z., Li, B., Hu, Q. L., and Gao, Q. J., "Dynamic Control Allocation Based on Robust Adaptive Backstepping Control for Attitude Maneuver of Spacecraft with Redundant Reaction Wheels," *24th Chinese Control and Decision Conference*, IEEE Publications, Piscataway, NJ, 2012, pp. 1354–1359.

[23] Schierman, J. D., Ward, D. G., Hull, J. R., Gandhi, N., Oppenheimer, M. W., and Doman, D. B., "Integrated Adaptive Guidance and Control for Re-Entry Vehicles with Flight-Test Results," *Journal of Guidance, Control, and Dynamics*, Vol. 27, No. 6, 2004, pp. 975–988. doi:10.2514/1.10344

[24] Zhang, Y. M., Suresh, V. S., Jiang, B., and Theilliol, D., "Reconfigurable Control Allocation Against Aircraft Control Effector Failures," *Proceedings of IEEE Conference on Control Applications*, IEEE Publications, Piscataway, NJ, 2007, pp. 1197–1202.

[25] Alwi, H., Edwards, C., Stroosma, O., and Mulder, J. A., "Fault Tolerant Sliding Mode Control Design with Piloted Simulator Evaluation," *Journal of Guidance, Control, and Dynamics*, Vol. 31, No. 5, 2008, pp. 1186–1201. doi:10.2514/1.35066

[26] Casavola, A., and Garone, E., "Fault-Tolerant Adaptive Control Allocation Schemes for Overactuated Systems," *International Journal of Robust and Nonlinear Control*, Vol. 20, No. 17, 2010, pp. 1958–1980. doi:10.1002/rnc.v20:17

[27] Page, A. B., and Steinberg, M. L., "Closed-Loop Comparison of Control Allocation Methods," *AIAA Guidance, Navigation and Control Conference*, AIAA, Reston, VA, 2000, pp. 1760–1770.

[28] Zhang, Y., and Chen, Z. J., "Closed-Loop Control Allocation Method for Satellite Precision Pointing," *IEEE 10th International Conference on Industrial Informatics*, IEEE Publications, Piscataway, NJ, 2012, pp. 1108–1112.

[29] Hughes, P. C., *Spacecraft Attitude Dynamics*, Wiley, New York, 2004, p. 59.

[30] Bodson, M., "Evaluation of Optimization Methods for Control Allocation," *Journal of Guidance, Control, and Dynamics*, Vol. 25, No. 4, 2002, pp. 703–711. doi:10.2514/2.4937

[31] Yildiz, Y., and Kolmanovsky, I., "Stability Properties and Cross-Coupling Performance of the Control Allocation Scheme CAPIO," *Journal of Guidance, Control, and Dynamics*, Vol. 34, No. 4, 2011, pp. 1190–1196. doi:10.2514/1.50310

[32] Golub, G. H., and Van Loan, C. F., *Matrix Computations*, Johns Hopkins Univ. Press, Baltimore, MD, 1996, pp. 46–57.

[33] Franklin, G. F., Workman, M. L., and Powell, D., *Digital Control of Dynamic Systems*, 3rd ed., Addison Wesley Longman, Reading, MA, 1997, pp. 47–52.

[34] Zhang, F., *Matrix Theory: Basic Results and Techniques*, Springer-Verlag, New York, 2011, pp. 67–71.